Development of High-power Infrared Laser Capable Phase-only Spatial Light Modulator

Yu Takiguchi*, Hiroshi Tanaka, Tsubasa Watanabe, Naoaki Kato, Keisuke Uchida, Munenori Takumi, Tomoko Otsu-Hyodo, Kazuhiro Nakamura, and Haruyoshi Toyoda

Central Research Laboratory, Hamamatsu Photonics K. K., Japan
Corresponding author's e-mail: takiguchi-y@crl.hpk.co.jp

We developed two types of liquid-crystal spatial light modulators: an improved device by modifying each layer of the device and a large active area for industrial infrared lasers to demonstrate innovative manufacturing and fabrication techniques in smart manufacturing. The reconstruction of computer-generated holograms was demonstrated to prove the concept of the proposed device in the IR region. The incident phase performance characteristics of the device under high-power laser irradiation were obtained using a 1030 nm ultrashort pulse laser.
DOI: 10.2961/jlmn.2023.03.2001
Keywords: additive manufacturing, digital photonics, holographic laser processing, spatial light modulator, ultrashort pulse laser processing

1. Introduction

The smart manufacturing concept based on the full use of Internet of Things (IoT) technologies has the potential to play an active role in the post-pandemic era, such as in failure prediction, defective product detection, human resource development, and energy saving. Among the emerging IoT technologies, laser processing has garnered considerable attention owing to its benefits of digital controllability, along with advances in the fourth industrial revolution [1,2]. Cyber-physical system (CPS) is also an analogical concept to smart manufacturing because these concepts share the same basic architecture, although a CPS has a higher combination and coordination between physical and computational elements, as detailed in the subsequent section. Dynamic beam shaping is one of the featured technologies to offer opportunities in temporal and/or spatial interaction between light and matters. There are several well-known devices such as grating light valves [3], deformable mirrors [4], and microelectromechanical systems (MEMS) [5] that can be used in high power laser processing. Among those techniques, active wavefront modulation technology using liquid-crystal-on-silicon spatial light modulators (LCOS-SLMs) is considered highly promising for next-generation optical laser processing systems in the post-pandemic era for its flexibility [6, 7]. However, the application field is limited by the power handling capability of LCOS-SLMs. In this paper, we introduce our recent developments in LCOS-SLMs, which can be classified into two steps: improvement of commercialized LCOS-SLMs by modifying each layer of the device and large active area LCOS-SLMs designed from scratch to improve the heat exhaust efficiency and suppress the peak power to reduce laser-induced damage. The former improvement is described in Section 3 whereas the latter in Section 4.

2. LCOS-SLMs for CPS laser processing systems

2.1 Basic concept of CPS with wavefront modulation

The CPS manufacturing system is a mechanism in which the cyberspace side optimizes the machine, where the factory performs each production process for the design drawings sent as data. It is described as part of the "super smart society", which is a practice proposed in "The 5th Science and Technology Basic Plan" by the Japanese government. The term super smart society refers to a human-centered society that balances economic advancement with the resolution of social problems using a system that integrates cyberspace and physical space. In other words, it is necessary to change from the current mass production to small-lot multi-production to realize a society in which necessary products and services can be obtained when required.

The versatility of laser processing, including application in machine processes such as drilling, cutting, welding, and additive manufacturing, makes it a highly attractive choice for on-demand production of various products. This can reduce the time, material, and labor costs. However, laser machining involves multiple scales in time and space of over ten digits from the start of irradiation to the end of processing. This indicates that high levels of performance are required for both cyber and physical systems to obtain an optimal solution under such circumstances, compared to other CPS systems. The difficulty in constructing cyberspace for laser machining is due to its high-order nonlinearity and non-equilibrium and irreversible processes. Cyberspace will serve as a platform for generating optimized receipts, and the big data stored as teacher data will be analyzed using artificial intelligence (AI) and theoretical and numerical simulations. The analysis results provide feedback on the physical space in various forms. Several strategies can be employed to build simulators by collecting a wide range of processing results using various parameters. These strategies mostly focus on applying big data to AI, such as deep learning, for advanced prediction of optimized parameter combinations. Collecting a wide range of processing results as deep learning teacher data is the most important task for realizing this cyberspace, highlighting the importance of a physical data acquisition laser pro-

cessing system for repeated experiments in terms of accuracy and throughput.

Accurate feedback analysis results from cyberspace need to be effectively implemented in the physical space. Arbitrary control of the time, frequency, and spatial domains is indispensable. Laser and light-source technologies have advanced significantly in the last decade, meeting most of the laser processing demands in the time and frequency domains. Wavefront control is expected to be a key technology in optical systems for maximizing the digital handling of laser-processing optics in the space domain. Most laser processing technologies focus on light with an objective lens, and the intensity distribution at the focal spot is directly related to the complex pupil function of the lens [8]. The complex pupil function can be written in polar coordinates using two real functions, namely the phase distribution changes introduced by the optics and the amplitude distribution, indicating that wavefront modulation exhibits a very high potential to act as a pupil function mask. The simultaneous realization of multibeam generation and aberration correction [9] can also improve the performance and quality of the system. Data acquisition using laser processing systems can be parallelized for high throughput by setting phase-only SLMs inside the data-acquisition laser processing system.

2.2 Overview of LCOS-SLMs

The advancement of phase-only SLMs enables real-time optical processing with a significantly high light utilization efficiency. For instance, adaptive optics, which is a typical example of a wavefront control application, can improve the stability of a laser source and the thermal aberrations induced in an optical system. Liquid crystal (LC)-based SLMs have been widely used, particularly for high spatial resolution and high stability applications. LCOS-SLMs, which are electrically addressed reflective-type SLMs with an LC, are suitable for wavefront control in industrial and medical applications because it is relatively easy to realize low-cost, small size, ease of handling, robustness against vibrations, and low-voltage driving devices.

Figure 1 shows the configuration of the LCOS-SLM device. The device consists of a glass substrate, a transparent electrode, two alignment layers, a parallel-aligned nematic LC layer, a multilayered dielectric mirror, and a silicon backplane on which an active-matrix circuit connected to pixelated metal electrodes was fabricated. A 3-mm thick optically flat glass plate was selected as the glass substrate to maintain flatness even after fabrication. A multilayered dielectric mirror was used to enhance reflectivity. Parallel alignment of the LC enabled pure phase modulation. The driver included a digital video interface (DVI) receiver such that users could use the device as an extra display on a computer. The input 8-bit digital signals from the DVI were converted to analog signals using 12-bit digital-to-analog converters in the driver after compensating for LC nonlinearity.

A multilayered dielectric mirror between the LC layer and the silicon backplane achieved high light utilization efficiency, which was defined as the ratio of the 0th order diffraction light intensity to the input light intensity. In addition, we adopted advanced CMOS technology to reduce the diffraction loss caused by the pixel structure. Consequently, a very high light utilization efficiency of over 90% was achieved, which is effective for laser processing applications and significantly weak optical signal detection.

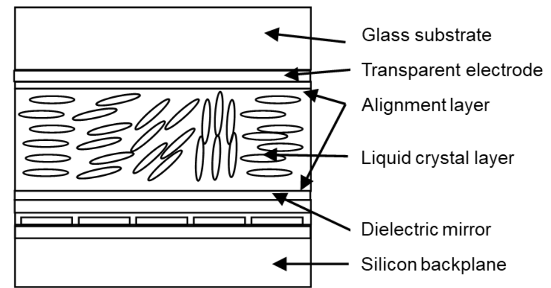

Fig. 1 Structure of the LCOS-SLM device.

3. Newly designed LCOS-SLMs for high-power laser resistance

3.1 Requirements of high-power laser resistance LCOS-SLMs

The properties of LCOS-SLMs change in several steps under high-power laser irradiation conditions, such as wavefront distortion with temperature changes, phase modulation malfunction mainly due to nonlinear optical effects, and direct laser-induced damage to constituent materials [10]. These phenomena occur in the order of the laser pulse intensity. The first two phenomena are reversible, indicating that by turning the irradiating laser off, the changes in distortion and phase modulation return to their original states. In the first step, our task was to achieve a threshold of reversible changes closer to the laser-induced damage threshold (LIDT). The irreversible changes are assumed to be limited by the physical properties of the constituent materials of LCOS-SLMs.

3.2 Optimization of dielectric mirror designing and LIDT testing with ultrashort pulse laser

A multilayered dielectric mirror between the LC layer and the silicon backplane (Fig. 1) enabled the achievement of a high light utilization efficiency. In a general multilayer design, two materials with different refractive indices are stacked alternately. A material with a high refractive index n_{high} was deposited onto the substrate with a thin layer and thicker layers with a lower refractive index n_{low}. This configuration resulted in a significantly high reflectance; however, a strong electric field intensity peak also occurred at the material boundaries inside the mirror. The threshold of the dielectric breakdown of n_{high} materials is typically lower than that of n_{low} materials [11]. If the intensity peaks shift slightly inside n_{high} materials, the dielectric mirror will be significantly damaged. To avoid such a concentration of the electric field intensity inside the high-refractive-index layers, we adopted an optimized aperiodic structure for several layers near the mirror surface. The thickness of the layers was modified to shift the peak position of the electric-field intensity inside the low-refractive-index material layers. This design concept reduced damage and ensured the high reflectivity of conventional designs. Figure 2 shows the electric field simulation of the newly designed dielectric mirror with shifted electric field intensity peaks compared with the conventional mirror design. The intensi-

ty peaks were successfully shifted inside the n_{low} material, corresponding to the odd number on the horizontal axis of Fig. 2, to avoid laser damage.

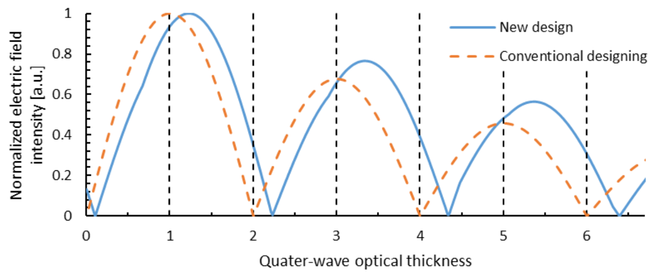

Fig. 2 Simulation of electric field intensity inside designed multilayered dielectric mirrors.

Multilayer dielectric mirrors were deposited through ion-beam-assisted deposition. Accelerated ions were irradiated toward the evaporated deposition target material to collide and deposit kinetic energy from the ions. The evaporated materials reached the substrate with high energy, and the density of each layer was increased to form a high-density film compared to the conventional vacuum deposition method. We measured the reflectance spectrum of a dielectric mirror designed for 1064 nm YAG lasers, demonstrating a reflectivity of over 99.9%. The reflectivity compared to the conventional design was identical, as shown in Fig. 3; an additional 0.05% improvement from 97.86 ± 0.02% to 97.91 ± 0.02% in average was observed in the 1000–1100 nm range.

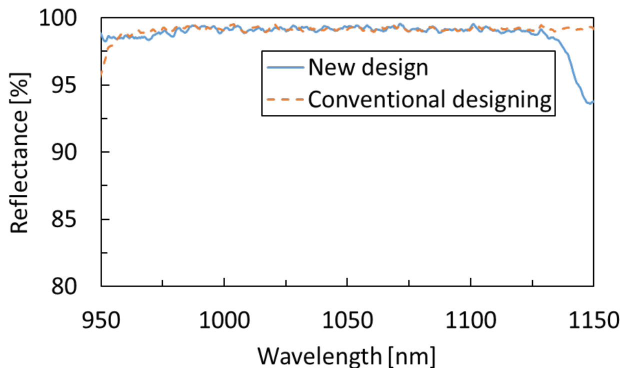

Fig. 3 Reflection properties of the new dielectric mirror.

The LIDT is defined in ISO 21254 as the "highest quantity of laser radiation incident on an optical component for which the extrapolated probability of damage is zero" [12]. We used a one-on-one method to evaluate the damage. A diode-pumped femtosecond industrial laser (Monaco 1035-80-60, Coherent Inc.) with a pulse duration of 262 fs (FWHM), central wavelength of 1030 nm, and repetition rate of 1 MHz was used to irradiate the samples. The sample mirror under the object lens was irradiated with a high-power laser, which gradually changed the fluence, and the damaged area was observed. Consequently, the LIDT of the newly designed mirror was improved from 4.0 J/cm^2 to 7.3 J/cm^2 compared to the conventional mirror design.

3.3 Prototype device

We redesigned each LCOS-SLM layer, as illustrated in Fig. 1, to reduce phase modulation malfunction. The material and deposition conditions of the transparent electrode were considered to have higher transparency in the near-infrared wavelength range. A multilayer was specified for a high-laser-power-resistance LCOS-SLM by shifting the peak wavelength and optimizing the outer layer thickness for a higher reflectance and LIDT, as explained in the previous section. A CMOS backplane was also designed to reduce nonlinear absorption by inserting light shielding layer below the electrodes.

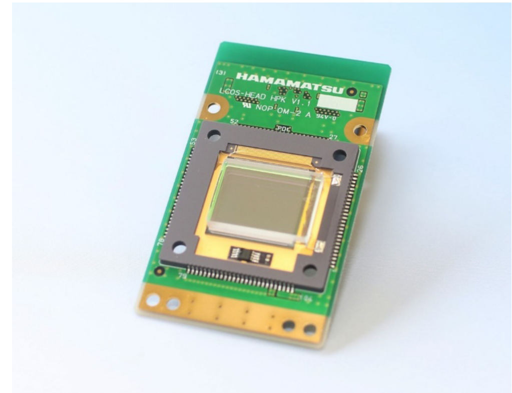

Fig. 4 Prototype LCOS-SLM with high laser power capability.

3.4 Experimental setup for phase measurement under high-power laser irradiation

To confirm the improvement of the LCOS-SLM to the phase-modulation malfunction, we measured the voltage-dependent birefringence of the device using a polarization interferometer [10, 13] while irradiating it with a high-power laser. Nematic LCs consisting of rod-like molecules were aligned in parallel in a horizontal orientation inside the device. When polarized monochromatic light propagated through a homogeneously aligned LC layer with a linear polarization axis at 45°, a phase difference occurred between the extraordinary and ordinary rays of the outgoing light. If the LC layer was placed between the polarizer and the analyzer set in a crossed Nicol configuration, the transmitted intensity was modulated according to phase changes.

Figure 5 shows the setup of the polarization interferometer. A continuous-wave 1064 nm-wavelength laser beam (Forte, Laser Quantum) was expanded to φ 10 mm in diameter after spatial filtering. The beam size of the femtosecond laser (1/e^2) was φ 3 mm at the surface of the LCOS-SLM. A high-pass filter was placed in the polarization interferometer to prevent light scattering from the pump laser. A water-cooling heat sink was attached to the device to minimize the effects of temperature changes, and the device temperature was monitored using a thermal camera. The drift of temperature was suppressed below ±2.0 °C throughout this experiment.

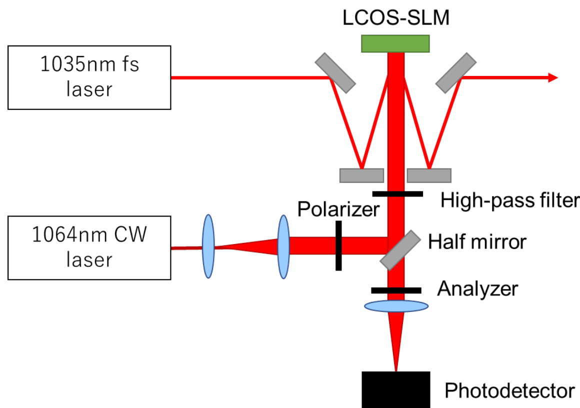

Fig. 5 Polarization interferometer for measuring the voltage-dependent birefringence of the device.

The total amount of phase modulation was determined as an indicator of phase modulation malfunction. We set this value as a 5% decrease from the initial total amount of phase modulation in the specific voltage range to achieve a 3π radian at 1030 nm. The 5% decrease corresponds to λ/30 wavefront distortion expression, i.e. strehl ratio over 0.95, which is a requirement for the LCOS-SLM to be applied to a precise CPS laser processing system in future. The intensity of the incident laser was increased stepwise, and the total phase modulation was measured using a polarization interferometer. Figure 6 shows the results, incident laser power on the horizontal axis, and the normalized total phase modulation on the vertical axis. Each data was taken after 10 minutes exposure with changed laser power which is sufficient time to ensure the stability both in temperature and device operation. We increased the maximum average power of the laser (60 W) and confirmed that a slight degradation occurred in the total amount of phase modulation, which was still below the threshold in our new device. After the irradiation with 60 W to the conventional device, we also measured the dynamic changes in total phase modulation immediately after shutting the laser off to confirm the effect of temperature. However, total amount of phase modulation quickly returns to initial value, which indicates that the thermal effect is not dominant in this laser power range. We believe nonlinear absorption inside the CMOS backplane mainly causes such malfunction.

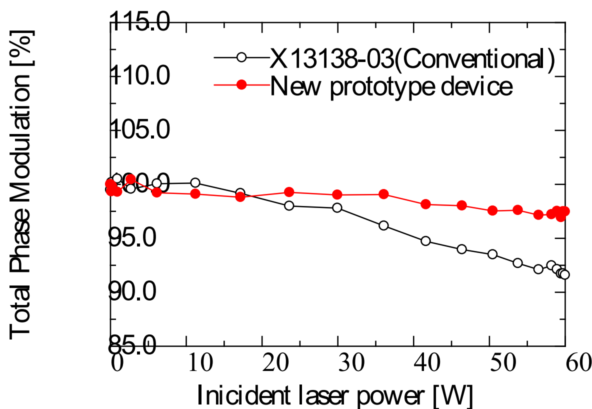

Fig. 6 Incident laser power dependency of total phase modulation.

3.5 Joint Application Lab at Fraunhofer ILT

A joint application lab was set up at Fraunhofer ILT with Hamamatsu Photonics [14]. They built an industry-ready prototype laser processing system to develop manufacturing processes. This included a scanner-based process head, in which a high-power LCOS-SLM was integrated. The head was integrated into a 3-axis machine with a 150 W ultrashort pulse laser. The Fraunhofer ILT team investigated surface and volume ablations using different beam profiles and focus diameters. The heat distribution in the workpiece becomes increasingly important when large average laser powers are applied, and the ultrashort pulse laser processes are scaled in speed and efficiency. Thus, the energy distribution and heat input within the parallelized beam distribution can be optimized. In the joint application lab, Fraunhofer ILT helps customers develop manufacturing processes. In addition, it uses the knowledge and technology developed in new research projects.

4. Development of large active area LCOS-SLMs

4.1 Basic concept of large active area LCOS-SLMs

The development of an LCOS-SLM with a large active area to reduce the peak power of incident light and for efficient cooling is another approach to achieve high-power laser capability, particularly for continuous wave (CW) laser applications. The task in this section was to create a silicon backplane and glass substrate with a 30.7 mm square.

Table 1 summarizes a comparison of the device specifications of the current LCOS-SLM device (X15213 series, Hamamatsu Photonics K.K.) and 30.7 mm of its active area. The fill factor was set at 96% to obtain the same value as that of the current device. The pixel size was four times larger than that of the current device, which was due to the suppression of the flyback region between the pixels with different supplied voltages. This flyback region is known to reduce first-order diffraction efficiency. Optical flatness of large area LCOS-SLM was manufactured to be below 1.0 lambda in root mean square at 1064 nm to be identical to conventional devices.

Tab. 1 Main specification of large area LCOS-SLM for infrared lasers.

Parameter	SLM of Sec. 3	Large area SLM
Wavelength (nm)	1050 (±50)	1050 (±50)
Number of pixels	1272 × 1024	1008 × 1024
Effective size (mm)	15.9 × 12.8	30.24 × 30.7
Pixel pitch (μm)	12.5	30.0
Aperture ratio (%)	96.8	96.7

4.2 Silicon backplane fabrication using the CMOS stitching technique

The stitching technique is a method of repeatedly exposing semiconductor circuits to a silicon substrate and was first demonstrated in CCD imagers [15]. The repetitive structure of the CMOS backplane was split into smaller blocks that could be exposed by steppers with smaller exposure areas than that of the backplane. This allows the fabrication of large-circuit patterns that cannot be entirely exposed simultaneously. The optimized design of such a

piece, a backplane of an arbitrary size, can be built from the same blocks to reduce the number of masks required. By applying stitching techniques, we instigated when we were developing and manufacturing large-area opto-semiconductors, we built the new SLM with an effective area of 30.24 mm × 30.7 mm, approximately 4 times larger than our previous device.

4.3 Prototyping of large active area LCOS-SLMs

Figure 7 shows two prototype devices: the redesigned LCOS-SLM described in Section 3 and one of the world's largest currently available liquid-crystal SLM, which effectively reduces the incident energy per unit area on the SLM [16]. These new SLMs also employ a large ceramic substrate with excellent heat resistance and thermal conductivity to improve heat dissipation efficiency. Our prototype device required a higher supply current owing to the size of the electrodes compared with conventional devices, and two flexible printed circuit cables were connected to the upper and lower connectors. An LCOS-SLM controller was also developed to meet this requirement. There was a minor temperature increase of this device up to 2 °C while operating, although this is also identical to conventional devices.

Typically, large-area silicon substrates are prone to warping and flatness deterioration during the manufacturing process, which distort the irradiation beam patterns and shapes. However, using our unique optosemiconductor manufacturing technology, we developed a technique that maintains substrate flatness while increasing the SLM effective area. This provides a beam shape that can be controlled with a high degree of accuracy.

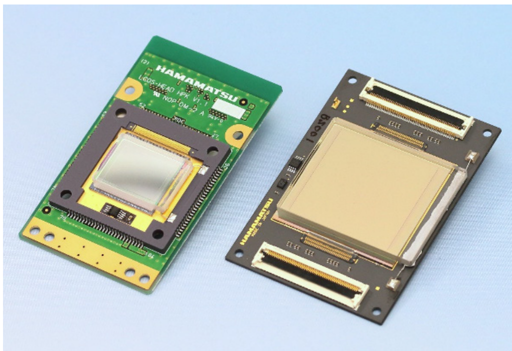

Fig. 7 Prototype LCOS-SLM described in Sec. 3 (left) and 30 mm square area device (right).

In general, the amount of phase modulation by the LC relative to the input voltage is nonlinear, and it uses a look-up table that linearly relates the phase modulation amount to a signal. The 12-bit signal was sent to an LCOS-SLM controller from a PC and subsequently converted to the input voltage by the controller. The phase modulation profile obtained after this correction is shown in Fig. 8. The linearity error was less than 0.03π radians, which is identical to comercialized devices.

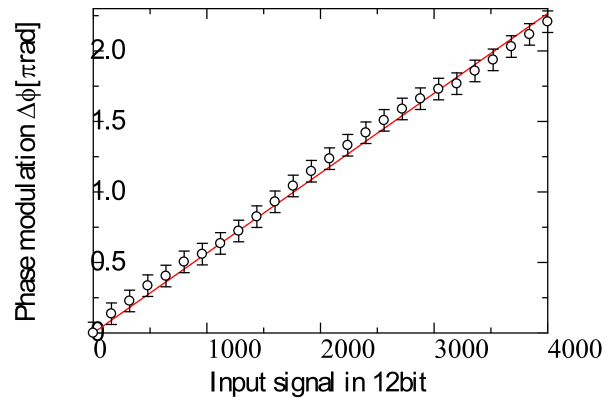

Fig. 8 Calibrated phase modulation.

We also demonstrated the performance of hologram reconstruction with a φ 25mm top-hatted 1064 nm CW laser by displaying a multi-spot hologram to the large-active-area LCOS-SLM. The generated beam pattern is monitored using a CMOS camera, as shown in Fig. 9. Because we did not implement correction of the wavefront distortion caused by the optical system and LCOS-SLM, each focal spot deviated from the perfect airy disk, which we will refine in the future. The remained power in 0th order was 2.9% with this hologram, which was slightly higher compare to comertialized devices.

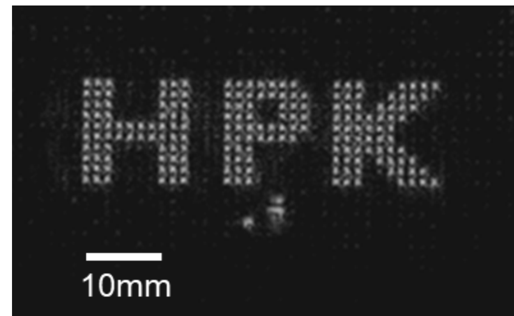

Fig. 9 Demonstration of holographic multi-spot generation with a large active area LCOS-SLM.

4.4 Experimental results under high-power fs laser irradiation

Using the polarization interferometer shown in Fig.5, we obtained the total phase modulation of a large-area LCOS-SLM. The beam size of femtosecond laser was φ 3 mm at the surface. Figure 10 shows the results, incident laser power on the horizontal axis, and the normalized total phase modulation on the vertical axis. We increased the power up to the maximum average value of the laser (60 W) and confirmed that a slight degradation in the total phase modulation amount occurred, which was still below the threshold, indicating that the laser power capability per area is identical to the improvements described in Section 3. The effective area is four times larger, and this large-area device has the potential to handle ultrashort-pulse lasers of 250 watts or higher.

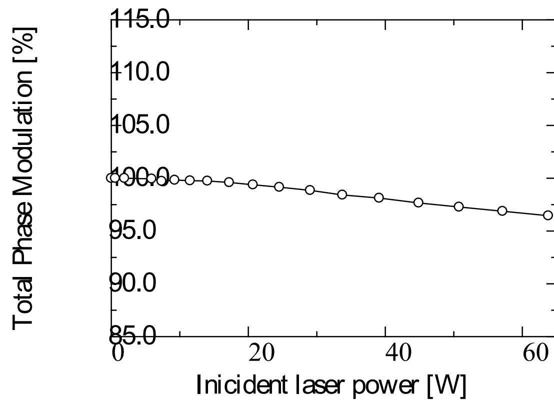

Fig. 10 Incident laser power dependency of total phase modulation (large active area LCOS-SLM).

5. Summary and conclusion

In summary, we reported two improved LCOS-SLM devices for handling high-power lasers in the infrared region. The experimental results indicated a high-pulse laser power capability for industrial applications. Our main objective was to demonstrate the concept of laser processing, including additive manufacturing with a CPS, as part of smart manufacturing. This research will help accelerate the use of LC SLMs for high-throughput, high-precision laser processing of resistant materials, such as lightweight and high-strength carbon fiber-reinforced plastics and low-k materials. We are making further progress in improving the light-resistance properties and installing a CPS-type laser processing system. Additionally, the combination of subtractive laser processing and additive manufacturing is one of the main targets for boosting laser-handling technologies in this field.

Large active area prototype LCOS-SLM (30.7 mm) also has the potential for higher heat dissipation from the larger back plate cooling configuration. It successfully suppressed the temperature increase that occurred during irradiation with a CW laser, making this LCOS-SLM ideal for high-power industrial CW laser systems. Using this new SLM in an industrial CW laser system for simultaneous multipoint processing will improve the laser thermal processing efficiency in laser welding, laser cutting tasks, and three-dimensional metal printing. Moreover, accurately controlling and optimizing the beam shape according to the material and shape of the object can provide a higher precision in laser thermal processing.

Acknowledgments

This study was partially supported by the Council for Science, Technology, and Innovation (CSTI), the cross-ministerial strategic innovation promotion program (SIP), "Photonics and Quantum Technology for Society 5.0" (funding agency: QST), the JSPS grant-in-aid for specially promoted research grant number JP16H06289, and AMED under grant number 21WM0525013H0001.

References

[1] W.M. Steen and J. Mazumder: "Laser Material Processing, 4th ed.," (Springer, London, 2010) p.485.
[2] A. Ustundag and E. Cevikcan: "Industry 4.0: Managing The Digital Transformation," (Springer, Cham, 2018) p.3.
[3] H. Matsui, T. Nagao, Y. Norimitsu, and S. Majima: J. Photopolym. Sci. Technol., 31, (2018) 463.
[4] L.D. Nair, C. Goppold, P. Böttner, D. Stoffel, A. Jahn, C. Jolliffe, and M. Bach: Lasers in Engineering, 46, (2020) 305.
[5] G. Zhou, Z.H. Lim, Y. Qi, F.S. Chau, and G. Zhou: Int. J. Optomechatronics, 15, (2021) 61.
[6] S. Hasegawa, Y. Hayasaki, and N. Nishida: Opt. Lett. 31, (2006) 1705.
[7] M. Silvennoinen, J. Kaakkunen, K. Paivasaari, and P. Vahimaa: Opt. Express, 22, (2014) 2603.
[8] J. W. Goodman: "Introduction to Fourier Optics, 3rd ed.," (Roberts & Company, Greenwood Village, 2005) p.107.
[9] Y. Takiguchi, M. Oyaizu, N. Makoto, T. Inoue, and H. Toyoda: Opt. Eng., 56, (2017) 077109.
[10]Y. Takiguchi, H. Tanaka, T. Tsubasa, H. Asaine, N. Mukozaka, Y. Ohtake, and H. Toyoda: Proc. SPIE, 11673, (2021) 1167305.
[11]P. W. Baumeister,:"Optical coating technology", (SPIE press, Bellingham, 2004) p. 3-41.
[12]ISO standard 21254-1, International Organization of Standardization, 2011
[13]S. T. Wu, U. Efron, and L.V.D. Hess: Appl. Opt., 23, (1984) 3911.
[14]Press release from Fraunhofer ILT, <https://www.ilt.fraunhofer.de/en/press/press-releases/2022/9-5-hamamatsu-slm-joint-application-lab.html>
[15]G. Kreider, J. Bosiers, B. Dillen, J. van der Heijden, W. Hoekstra, A. Kleimann, P. Opmeer, J. Oppers, H. Peek, R. Pellens, and A. Theuwissen: IEDM Technical Digest, (1995) 155.
[16]H. Tanaka, Y. Takiguchi, T. Watanabe, N. Kato, K. Uchida, T. Munenori, T.O. Hyodo, K. Nakamura, H. Ishii, A. Ihori, Y. Akizawa, H. Asaine, M. Nagata, Y. Ohtake, and H. Toyoda: Proc. SPIE, 12442 (2023) 12442-16.

(Received: June 9, 2023, Accepted: September 30, 2023)